Actively controlled cardiac afterload

Pigot, Harry; Wahlquist, Ylva; Soltesz, Kristian

Published in:
IFAC Proceedings Volumes (IFAC-PapersOnline)

2023

Document Version:
Peer reviewed version (aka post-print)

Actively controlled cardiac afterload

Henry Pigot * **Ylva Wahlquist** * **Kristian Soltesz** *

* *Lund University, Dept. Automatic Control, Sweden*
*(e-mail: {*first.last*}@control.lth.se)*

Abstract: *Ex vivo* (outside of the body) working heart models enable the evaluation of isolated hearts. They are envisioned to play an important role in increasing the currently low utilization rate of donor hearts for transplantation. For the heart to work in isolation, an afterload (flow impedance) is needed. To date, afterload devices have been constructed by combining multiple constituent elements such as pumps, flow resistances, and flow capacitances (compliances), typically to replicate the structure of so-called Windkessel models. This limits active control to that achievable by varying these elements, making it slow and subject to the problem of dynamic coupling between parameters. Here we present a novel concept to achieve Windkessel dynamics through a very simple variable flow impedance. The impedance is actively controlled using feedback from a pressure measurement. Through simulations we demonstrate the ability to perfectly emulate Windkessel dynamics, while imposing tight pressure limits needed for safe operation—something not achievable with the verbatim implementation using constituent elements.

Keywords: Artificial organ, physiological modelling, control of physiological and clinical variables

1. INTRODUCTION

Ex vivo working heart models enable the organ to be studied in isolation from other physiological systems. In addition to being a valuable tool in basic physiology and pharmacology research, such models show potential for use in functional evaluation of donor organs prior to transplantation, as described by White et al. (2018); Gellner et al. (2020a). Functional evaluation may facilitate the safe use of organs from marginal donors—organs that would otherwise go unused—by providing clinicians with concrete evidence of organ performance, thereby expanding the organ donor pool.

Cardiac afterload is the impedance the body poses to blood flow from the beating heart. *Ex vivo* working heart models rely on devices that emulate this load. Ideally, a cardiac afterload device mimics physiological afterload while also enabling beat-to-beat control of arterial pressure—pulmonary artery pressure, if used with the right side of the heart, or aortic pressure if used with the left side. Ensuring that arterial pressure remains between prescribed limits is critical for the safety of the organ under test. When beating outside of the body, the heart lacks the protective pleura that otherwise prevents overextension of the ventricle in the event of high arterial pressures. Similarly, it is necessary to maintain a lower bound on aortic pressures to ensure sufficient perfusion of the coronary arteries during diastole despite variations in heart performance. These two factors make beat-to-beat control of cardiac afterload particularly important in *ex vivo* working heart models.

Cardiac afterload devices traditionally take one of two forms: a verbatim implementation of the common Windkessel lumped parameter models made up of discrete resistive and compliant elements as in Westerhof et al. (1971); Gellner et al. (2020b), described further in section 2.2, or as a fixed resistive element supplemented by a centrifugal pump attached to the artery as in White et al. (2015). The latter are capable of maintaining a lower bound on diastolic aortic pressure as set by the pump speed, while systolic pressures are dependent on the geometry of the

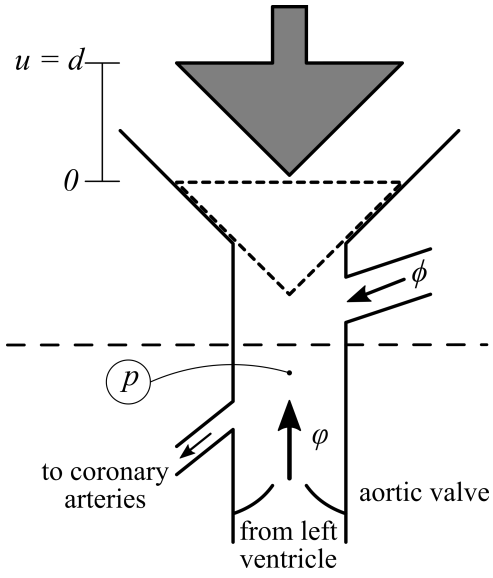

Fig. 1. Schematic of the afterload mechanism (above dashed line) connected to the heart (below). The afterload consists of a plunger actively controlled to position $0 < u \leq d$. The flow through the device consists of the aortic flow φ, and an auxiliary contribution ϕ, chosen to ensure $\phi + \varphi > 0$. Plunger position control is based on measurements of aortic pressure p.

afterload. Windkessel-based afterload designs rely on the tuning of resistive and compliant elements to set diastolic and systolic pressures. However, the parameters in both these afterload concepts are only slowly adjustable, such as in Fisher et al. (1984); Hatami et al. (2019); Gellner et al. (2020b), and the parameters are inherently coupled, making them unsuitable for beat-to-beat control of arterial pressures.

In Pigot et al. (2022), a novel nonlinear afterload concept was introduced. The concept is based on a variable compliance chamber that enables diastolic and systolic limit control. Here, we propose a more versatile, actively controlled afterload concept designed to mimic physiological afterload and provide beat-to-beat arterial pressure control. The use of feedback control enables a much simpler operating principle, consisting of a constant flow source and variable flow conductance controlled at high bandwidth relative to hemodynamics. We describe the variable-conductance concept using first-principles models and provide a control strategy to emulate common afterload models with the addition of pressure limits. We then investigate the afterload concept using simulation.

2. METHOD

2.1 Variable-conductance afterload

We want to control a dynamic aortic flow impedance using a variable flow conductance. An ideal, time variable, flow conductor relates aortic pressure p to aortic volumetric flow φ through Ohm's law

$$p = \frac{\varphi}{Y}, \tag{1}$$

where the conductance Y is the reciprocal of the resistance $R = Y^{-1}$.

The conductance is varied by moving a plunger that changes the flow path cross section area between some small—but non-zero—minimum value and some larger maximal value, as shown in Figure 1. The plunger is designed so that its position u is directly proportional to the conductance throughout its range of motion $0 < u \leq d$:

$$Y = Y_0 \frac{u}{d} > 0. \tag{2}$$

While the heart is viewed as a flow source in the Windkessel model literature, see Westerhof et al. (2009), it is arguably more physiologically correct to consider it as a power source as discussed by Pigot and Soltesz (2022), providing a time-varying instantaneous power profile

$$w = p\varphi. \tag{3}$$

In normal physiology, a flow reversal can occur at the beginning of diastole, just before the aortic valve closes, after which the diastolic aortic pressure facilitates coronary perfusion until the start of systole. The coronary flow is small relative to total cardiac output, and thus not explicitly modeled in the Windkessel literature. From (2) we get that $u > 0 \Rightarrow Y > 0$. Taking this into account, (1) dictates $p < 0$ whenever $\varphi < 0$ (being the case during flow reversal) while $u > 0$. A problem with this is that unlike the arterial vasculature that can provide a reverse flow thanks to its compliance, our plunger cannot. To eliminate this problem, a mechanically forced auxiliary perfusate feed flow ϕ is introduced between the heart and the variable conductance, as schematically illustrated in Figure 1.

With the auxiliary flow in place, our conductance model (1) is extended into

$$p = \frac{\varphi + \phi}{Y}. \tag{4}$$

The auxiliary flow rate ϕ needs to be sufficiently large to ensure a positive aortic pressure. Let $w_{\min}$ be the smallest expectable instantaneous power. If $w_{\min} \geq 0$, we can omit the auxiliary flow and thus set $\phi = 0$. Otherwise, combining (3) and (4), we can write

$$pY = \frac{w}{p} + \phi. \tag{5}$$

Knowing that $Y > 0$, we can re-write (5) as

$$p^2 - \frac{\phi}{Y} p - \frac{w}{Y} = 0 \tag{6}$$

with solutions

$$p = \frac{\phi}{2Y} \pm \sqrt{\left(\frac{\phi}{2Y}\right)^2 + \frac{w}{Y}}. \tag{7}$$

There thus exists a positive real solution p if and only if

$$\frac{\phi^2}{4Y^2} + \frac{w}{Y} > 0. \tag{8}$$

Since $Y > 0$ according to (2), the condition (8) can equivalently be written

$$\phi^2 + 4wY > 0. \tag{9}$$

The case requiring the largest ϕ thus occurs when $-wY$ is maximal. Letting $w_{\min} < 0$ denote the smallest expected power, the worst case condition occurs at $w_{\min} Y_0$, making

$$\phi \geq 2\sqrt{-w_{\min} Y_0} \tag{10}$$

sufficient. Note, however, that (10) is only a necessary condition if $w_{\min}$ is attained while $Y = Y_0$.

2.2 Emulating dynamics

Linear time-invariant reference dynamics Our objective is to actively control the position u of the plunger in Figure 1 to emulate desired dynamics between aortic pressure p and flow φ. In a realistic scenario one could measure the aortic pressure p with either a sensor in the perfusate stream, or—knowing the plunger cross section area—by the force by which the perfusate pushes onto the plunger. However, accurate direct measurements of aortic flow φ or instantaneous cardiac power w at a sample rate matching the time scale of the involved cardiac dynamics (at least tens of Hertz) remain elusive. We will circumvent the need for such measurements, through using the combined actuation model of (4) and (2) as a very simple soft sensor providing an estimate

$$\varphi = \frac{Y_0}{d} up - \phi. \tag{11}$$

In (11) we use the same notation for measured and actual pressure, as well as for estimated and actual flow. This brings us to a set of assumptions that we make:

- Disturbances acting on the pressure measurement and plunger position control are negligible.
- Discrepancies between the plunger model (2) and the dynamics of the device implementing it are negligible. This allows us to utilize (2) in (11).

- Delay between obtaining a new pressure sample and updating plunger position is negligible. This allows us to update plunger position instantaneously based on fresh pressure measurements.
- The plunger can be moved fast compared to the time scale of the (cardiac) dynamics that the system is to emulate. This allows us to assume that there are no dynamics between change of plunger position reference and actual plunger position u.
- Pressure is equitemporally sampled at a constant rate h that is sufficiently faster than the emulated dynamics, and slower than the plunger position dynamics. This means that w does not change notably between consecutive sampling instances.
- The auxiliary flow ϕ is controlled to a known constant level, such that $\varphi+\phi > 0$, or equivalently by (4) $p > 0$ is maintained at every instance.
- Historic pressure-flow data are consistent with the reference dynamics. This means that it is sufficient for us to maintain this consistency from one sample to the next in order to perfectly track the reference dynamics.

We deem it realistic to approximate the above assumptions related to modeling and measurement well through adequate hardware design, and discuss the topic further in section 4.

Let the reference dynamics that we wish to emulate be expressed through a continuous-time transfer function $G(s)$ (such as a Windkessel model) from aortic flow φ to pressure p. Zero-order-hold sampling of G at rate h, and subsequently applying the inverse z-transform then produces a difference equation

$$p_k = H(q^{-1})\varphi_k, \tag{12}$$

where subscript k indicates the time $t = kh$, so that for instance $p_k = p(kh)$, and where q^{-1} is the backward shift operator such that $q^{-m}p_k = p_{k-m}$.

If G is of order n, H can be parameterized as

$$H(q^{-1}) = \frac{b_0 + b_1 q^{-1} + \ldots + b_n q^{-n}}{1 + a_1 q^{-1} + \ldots + a_n q^{-n}}, \tag{13}$$

As a consequence of zero-order-hold sampling, there is no approximation error associated with (13) at the sampling instances. The constant coefficients b_k and a_k of (13) can be numerically (and in some cases analytically) determined based on G and h as described in for example Åström and Wittenmark (2011), and thus assumed to be known to us. For future convenience we also introduce the notation

$$B_1(q^{-1}) = b_1 q^{-1} + \ldots + b_n q^{-n}, \tag{14a}$$
$$A_1(q^{-1}) = a_1 q^{-1} + \ldots + a_n q^{-n}, \tag{14b}$$

that enable us to write

$$H(q^{-1}) = \frac{b_0 + B_1(q^{-1})}{1 + A_1(q^{-1})}. \tag{15}$$

Let $\tilde{p}_k$ denote the pressure measurement sampled at time $t = kh$, calculated in simulation using (7). We use (3) and (11) to reconstruct the (directly immeasurable) instantaneous power

$$w_k = \tilde{p}_k\tilde{\varphi}_k = \tilde{p}_k\left(\frac{Y_0}{d}u_k\tilde{p}_k - \phi\right). \tag{16}$$

where $\tilde{\varphi}_k$ is the actuation-model-based flow corresponding to $\tilde{p}_k$.

If (13) lacks direct term, signified by $b_0 = 0$, we can—assuming as stated above that we have historically matched the reference dynamics—solve for the pressure

$$p_k = \underbrace{B_1(q^{-1})\varphi_k - A_1(q^{-1})p_k}_{c_k}. \tag{17}$$

The right-hand-side, denoted c_k can be considered known at sampling instance k, since $A_1(q^{-1})p_k$ is a known linear combination of previously computed pressures, while $B_1(q^{-1})\varphi_k = B_1(q^{-1})(w_k/p_k)$ only relies on previously computed pressures and reconstructed instantaneous powers. One can note that in order for the reference dynamics to be trackable, it is required that $c_k > 0$. We will not go into details of analysing conditions for this, but suffice it to conclude that any reasonable LTI system (such as a Windkessel model) intended to describe the dynamics between aortic flow φ and pressure p will stay in the regimen of $p > 0$.

Thus p_k is known and the plunger can be moved to a new position u_k that is consistent with both the reconstructed instantaneous power w_k of (16) and the aortic pressure p_k of (17) dictated by the reference dynamics. This is done by combining (5) and (2), resulting in

$$u_k = \frac{d}{Y_0 p_k}\left(\frac{w_k}{p_k} + \phi\right). \tag{18}$$

If there is a direct term, signified by $b_0 \neq 0$, (13) instead gives us

$$p_k - b_0\varphi_k = \underbrace{B_1(q^{-1})\varphi_k - A_1(q^{-1})p_k}_{c_k}, \tag{19}$$

where c_k is the same as in (17) and thus can be considered known. Using (3) we can eliminate φ_k from (19) and arrive at the quadratic equation

$$p_k^2 - c_k p_k - b_0 w_k = 0 \tag{20}$$

with solutions

$$p_k = \frac{c_k}{2} \pm \sqrt{\frac{c_k^2}{4} + b_0 w_k}. \tag{21}$$

In order to honor continuity of the pressure profile, the positive solution that minimizes $p_k - p_{k-1}$ is chosen. We may also note that the solutions of (21) turn complex when $c_k^2 + 4b_0 w_k < 0$. For the concerned Windkessel models it holds that $b_0 \geq 0$, leading to complex solutions if and only if $w_k < -c_k^2/(4b_0)$.

As in the case without direct term, the computed reference pressure p_k is used to update the plunger position from u_{k-1} to u_k according to (18). This procedure is then repeated each time a new pressure measurement sample arrives.

Enforcing pressure limits Pressure limits can be imposed to ensure that the aortic pressure p remains within a safe span $p_{\min} \leq p \leq p_{\max}$. A simple way to achieve this is to clamp p_k to this span before applying (18). Doing so will of course violate the dynamics whenever the limits are active, but provide a practically feasible alternative to online adjustment of Windkessel model parameters to maintain pressure limits in presence of *e.g.* arrythmic events, as

illustrated later in section 3. Note that the Windkessel state (p,φ) must be tracked during clamping so as not to disrupt the desired dynamics.

Two-element Windkessel model Starting with the simplest Windkessel model, made up of two elements as described in Frank (1899); Westerhof et al. (2009), the dynamics from flow to pressure are expressed by the transfer function

$$G(s) = \frac{R_p}{1 + CR_p s}. \tag{22}$$

Zero-order-hold discretization and subsequent application of the inverse z transform, as outlined in section 2.2, yields

$$H(q) = \frac{b_0 + b_1 q^{-1}}{1 + a_1 q^{-1}}, \tag{23}$$

where

$$\begin{aligned} b_0 &= 0, \\ b_1 &= R_p\,(1 - \tau_1)\,, \\ a_1 &= -\tau_1, \end{aligned}$$

and

$$\tau_1 = e^{-h/(CR_p)}.$$

The lack of direct term means that we can employ (17) with

$$c_k = R_p\,(1 - \tau_1)\,q^{-1}\varphi_k + \tau_1 q^{-1} p_k. \tag{24}$$

Four-element Windkessel model Similarly, the 4-element Windkessel model as described in Deswysen et al. (1980); Westerhof et al. (2009) is expressed by the transfer function

$$G(s) = R_c + \frac{R_p}{1 + CR_p s} - \frac{R_c}{1 + L/R_c s}. \tag{25}$$

The zero-order-hold discretized version has the structure

$$H(q^{-1}) = \frac{b_0 + b_1 q^{-1} + b_2 q^{-2}}{1 + a_1 q^{-1} + a_2 q^{-2}}, \tag{26}$$

where

$$\begin{aligned} b_0 &= R_c, \\ b_1 &= R_p - R_c - \tau_1(R_p + R_c), \\ b_2 &= R_c\tau_1 - R_p\tau_2 + R_p\tau_1\tau_2, \\ a_1 &= -\tau_1 - \tau_2, \\ a_2 &= \tau_1\tau_2, \end{aligned}$$

and

$$\tau_2 = e^{-R_c h/L}.$$

The presence of direct term means that we can employ (21) with

$$c_k = \left(b_1 q^{-1} + b_2 q^{-2}\right)\varphi_k - \left(a_1 q^{-1} + a_2 q^{-2}\right) p_k. \tag{27}$$

2.3 Simulation examples

Simulations were performed to emulate 2- and 4-element Windkessel dynamics, with and without pressure limiting. The simulations were implemented in Julia, and the code and data used to generate the results published here are available on GitHub, see Pigot (2023). Measured human aortic volumetric flow from Stergiopulos et al. (1999) was used as input to discretized Windkessel models with parameters fit to the corresponding human aortic pressure measurements as described in Pigot et al. (2021), provided in Table 1. Both data sampling and model discretization were done with period $h = 5$ ms. The product of the input flow and resulting pressures from each model were used as the driving cardiac power for the respective simulations.

Table 1. Windkessel model parameters used in the simulations.

Model	R_p $\frac{\text{mmHg}}{\text{L/min}}$	C $\frac{\text{L}}{\text{mmHg}}$	R_c $\frac{\text{mmHg}}{\text{L/min}}$	L $\frac{\text{mmHg}\cdot\text{min}}{\text{L/min}}$
2-element	13.6	0.0996		
4-element	13.6	0.0743	0.952	0.0952

Maximum plunger displacement d was set to 3 cm, and maximum conductance $Y_0 = 0.9$ (L/min)/mmHg was tuned heuristically to yield displacements within this range. The lower bound $\phi \geq 49.6$ L/min given by (10) (for the 2-element model) is very conservative in practice, since w_{min} does not correspond to the fully open plunger position where $Y = Y_0$. Therefore, ϕ was set heuristically to a value below that, 21 L/min. The initial plunger position was set to $u = d/2$ to generate the first p and φ values used for plunger position control, which avoids excessive loading of the heart during startup. After several beats, transient behavior caused by the initial conditions dies out and the simulation reaches steady-state. The simulation results reported in section 3 show the last two of 20 cardiac cycles, long after initial condition transients become negligible.

3. RESULTS

Figures 2 and 3 show afterload simulations where the plunger position is actively controlled to replicate the 2- and 4-element Windkessel dynamics in Table 1, respectively. The plots illustrate simulation with (blue, solid) and without (red, dashed) upper and lower pressure limits on aortic pressure p. The limits were set to 80 and 105 mmHg for illustrative purposes, though a wider range of admissible pressures would generally be considered.

Practical examples of pressure-limiting are shown in Figures 4 and 5, where two arrythmic events are simulated with pressure limits set at 50 and 120 mmHg using the the 4-element Windkessel dynamics in Table 1. In Figure 4 the third beat occurs early (shifted back by 70% of the cardiac period), as in Pigot and Soltesz (2022), causing the upper limit to be enforced. To illustrate the lower limit, the second beat in Figure 5 is delayed by one cardiac period.

In all mentioned examples, the afterload simulations without pressure limits resulted in p and φ that are indistinguishable from the corresponding discrete-time Windkessel model simulations (error less than single precision machine epsilon). The pressure-limit-imposed differences in aortic flow in Figures 2 and 3 appear subtle compared to the differences in pressure. This is due to the differences between the minimum and maximum values; the differences in pressure appear clearer as it is plotted from 70 mmHg to 110 mmHg while flow is plotted from −5 L/min to 30 L/min.

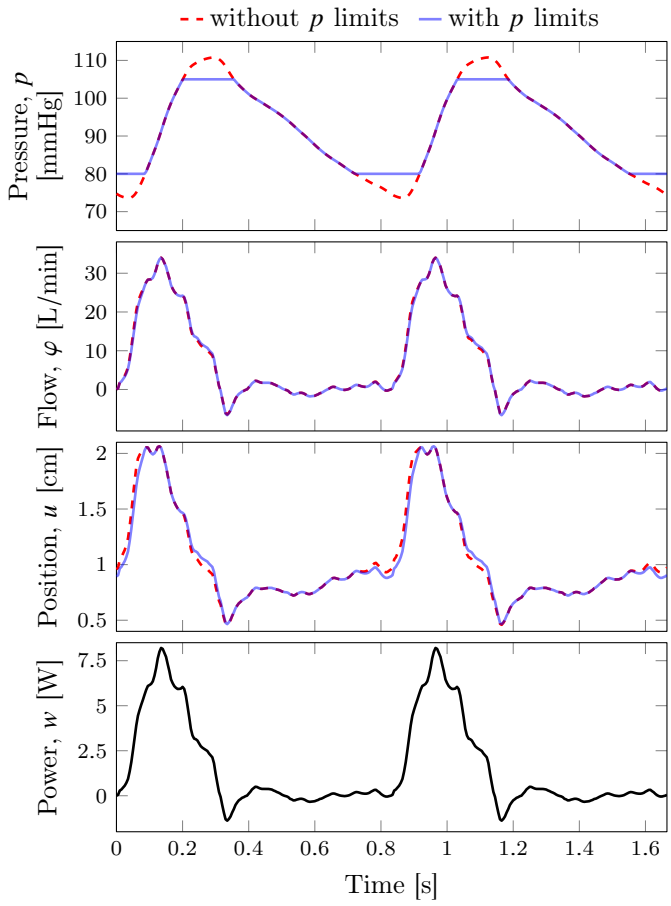

Fig. 2. Afterload simulation with plunger position u actively controlled to replicate 2-element Windkessel dynamics with (blue, solid) and without (red, dashed) limits on aortic pressure p, driven by cardiac power w. The limits are 80 and 105 mmHg. The resulting p and φ without limits are indistinguishable from the 2-element Windkessel model simulation.

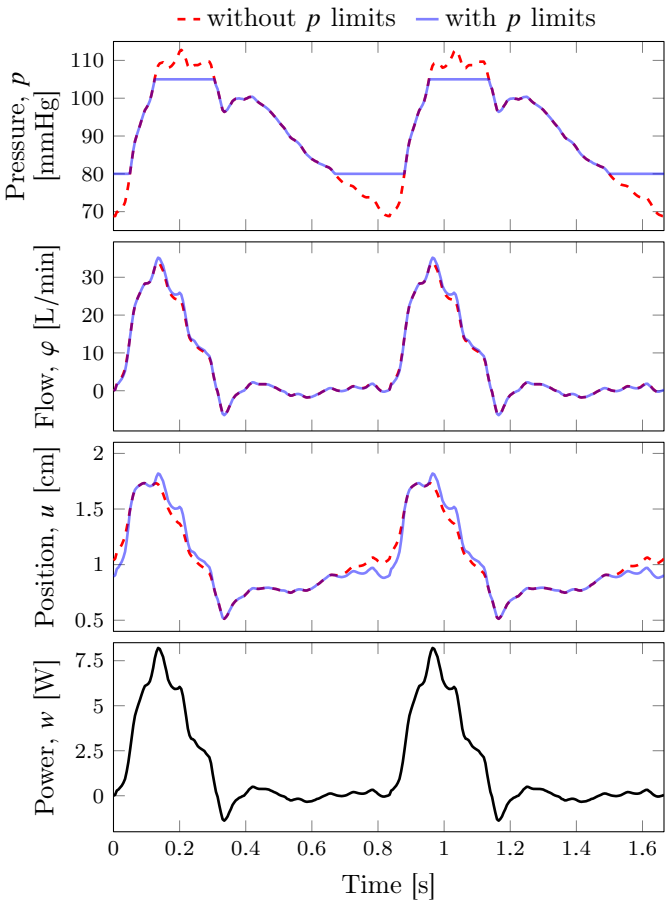

Fig. 3. Afterload simulation with plunger position u actively controlled to replicate 4-element Windkessel dynamics with (blue, solid) and without (red, dashed) limits on aortic pressure p, driven by cardiac power w. The limits are 80 and 105 mmHg. The resulting p and φ without limits are indistinguishable from the 4-element Windkessel model simulation.

4. DISCUSSION

The method presented here illustrates that it is in principle possible to replicate a wide range of dynamics relating pressure and flow, using the proposed afterload concept with auxiliary flow, schematically illustrated in Figure 1. However, in a viable implementation, the assumption made in section 2.2 would require explicit attention. There will for example be noise on the pressure measurement $\tilde{p}$, and inaccuracies in the actuation model (2). Investigating the impact of deviations from the assumptions will be a central part of future work. A simple way would be to introduce stochastic noise models, such as additive or multiplicative Gaussian noise to the simulation and investigate the impact of its variance on tracking performance. To get a better understanding of where in the cardiac cycle the system is most sensitive to measurement noise one could instead assume perfect tracking up to sample k, then compute and plot $\partial(p_k - p_k^*)/\partial\tilde{p}_k$, where p_k^* is the pressure corresponding to the updated plunger position, based the noise-free measurement $\tilde{p}_k^*$, while p_k is the corresponding pressure that would arise if the measurement was instead $\tilde{p}_k$. Similar analyses can be conducted to map out the impact of actuation model inaccuracies. However, it can be expected that they are more difficult to accurately characterize than the pressure measurement noise. Depending on the outcome of the analyses mentioned above, it might be necessary to de-tune tracking performance to reduce sensitivities to these deviations from the assumptions.

When first attaching a cardioplegic heart to the afterload system, it could be set to a constant pressure target. In this mode, the afterload would provide a flow-controlled constant pressure source to perfuse the coronary arteries—so called Langendorff mode perfusion, see Langendorff (1895)—wherein any perfusate not entering the coronary arteries would be shunted through the afterload, as evidenced by the illustration in Figure 1. After the resumption of normal cardiac rhythm, the afterload dynamics could be controlled to the desired dynamics, such as 4-element Windkessel with pressure limits. Our aim is to perform such tests in large animal experiments using hearts procured from pigs. A cyber-physical implementation of mechanism of Figure 1 has been constructed. Experiments are planned to commence shortly, once the prototype has undergone dry run tests.

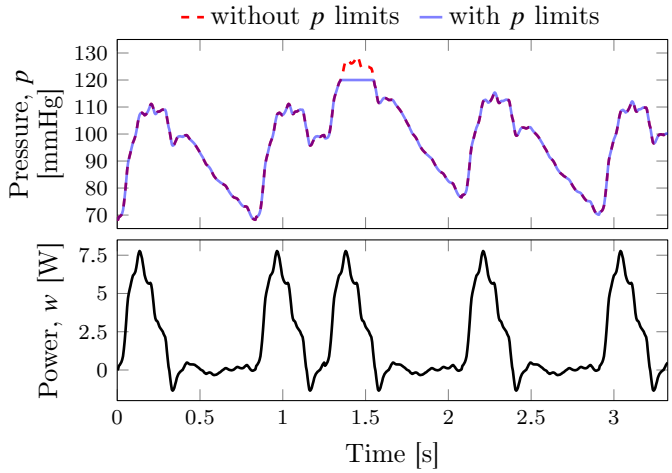

Fig. 4. Afterload simulation with the third beat shifted back by 70% of the beat period. The afterload is controlled to replicate 4-element Windkessel dynamics with (blue, solid) and without (red, dashed) limits on aortic pressure p, with limits set to 50 and 120 mmHg.

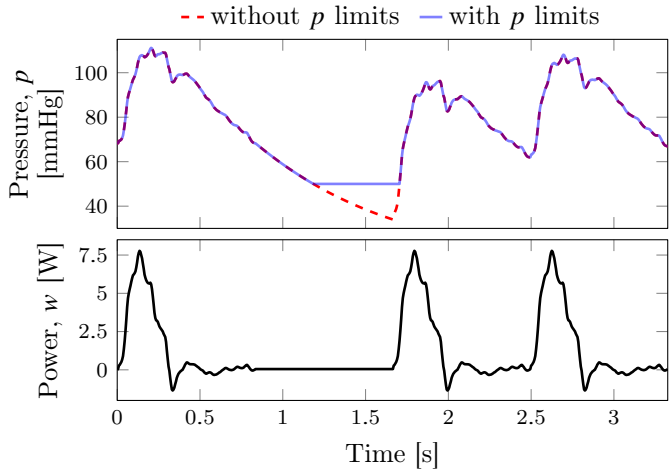

Fig. 5. Afterload simulation with the second beat delayed by one beat period. The afterload is controlled to replicate 4-element Windkessel dynamics with (blue, solid) and without (red, dashed) limits on aortic pressure p, with limits set to 50 and 120 mmHg.

5. ACKNOWLEDGEMENTS

This research was funded by the Swedish Research Council (grant 2017-04989), the Swedish Foundation for Strategic Research (grant SM21-0037), the Hans-Gabriel and Alice Trolle-Wachtmeister foundation, and the ELLIIT Strategic Research Area. We extend special thanks to our collaborators with the Division of Thoracic Surgery at Lund University, in particular Stig Steen and Trygve Sjöberg.

REFERENCES

Åström, K.J. and Wittenmark, B. (2011). *Computer-Controlled Systems: Theory and Design, Third Edition*. Dover Publications, Mineola, N.Y.

Deswysen, B., Charlier, A.A., and Gevers, M. (1980). Quantitative evaluation of the systemic arterial bed by parameter estimation of a simple model. *Medical and Biological Engineering and Computing*, 18(2), 153–166. doi:10.1007/BF02443290.

Fisher, A., Challis, R.E., and Swann, P. (1984). A controllable artificial afterload for isolated heart studies. *Journal of Biomedical Engineering*, 6(4), 305–310. doi:10.1016/0141-5425(84)90080-3.

Frank, O. (1899). Die Grundform des arteriellen pulses. *Zeitschrift für Biologie*, (37), 485–526.

Gellner, B., Xin, L., Pinto Ribeiro, R.V., et al. (2020a). The implementation of physiological afterload during ex situ heart perfusion augments prediction of post-transplant function. *American Journal of Physiology. Heart and Circulatory Physiology*, 318(1), H25–H33. doi:10.1152/ajpheart.00427.2019.

Gellner, B., Xin, L., Ribeiro, R.V., et al. (2020b). The Implementation of an Adjustable Afterload Module for Ex Situ Heart Perfusion. *Cardiovascular Engineering and Technology*, 11(1), 96–110. doi:10.1007/s13239-019-00447-w.

Hatami, S., White, C.W., Ondrus, M., et al. (2019). Normothermic Ex Situ Heart Perfusion in Working Mode: Assessment of Cardiac Function and Metabolism. *JoVE (Journal of Visualized Experiments)*, (143), e58430. doi:10.3791/58430.

Langendorff, O. (1895). Untersuchungen am überlebenden Säugethierherzen. *Archiv für die gesamte Physiologie des Menschen und der Tiere*, 61(6), 291–332. doi:10.1007/BF01812150.

Pigot, H. and Soltesz, K. (2022). The Differential-Algebraic Windkessel Model with Power As Input. In *American Control Conference, 2022 (in press)*. IEEE - Institute of Electrical and Electronics Engineers Inc.

Pigot, H. (2023). Actively controlled cardiac afterload simulation. URL `https://github.com/hpigot/controlled-cardiac-afterload`.

Pigot, H., Hansson, J., Paskevicius, A., et al. (2021). Identification of cardiac afterload dynamics from data. *IFAC-PapersOnLine*, 54(15), 508–513. doi:10.1016/j.ifacol.2021.10.307.

Pigot, H., Soltesz, K., Paskevicius, A., et al. (2022). A novel nonlinear afterload for ex vivo heart evaluation: Porcine experimental results. *Artificial Organs*, 46(9), 1794–1803. doi:10.1111/aor.14307.

Stergiopulos, N., Westerhof, B.E., and Westerhof, N. (1999). Total arterial inertance as the fourth element of the windkessel model. *American Journal of Physiology-Heart and Circulatory Physiology*, 276(1), H81–H88. doi:10.1152/ajpheart.1999.276.1.H81.

Westerhof, N., Elzinga, G., and Sipkema, P. (1971). An artificial arterial system for pumping hearts. *Journal of Applied Physiology*, 31(5), 776–781. doi:10.1152/jappl.1971.31.5.776.

Westerhof, N., Lankhaar, J.W., and Westerhof, B.E. (2009). The arterial Windkessel. *Medical & Biological Engineering & Computing*, 47(2), 131–141. doi:10.1007/s11517-008-0359-2.

White, C.W., Ambrose, E., Müller, A., et al. (2015). Assessment of donor heart viability during ex vivo heart perfusion. *Canadian Journal of Physiology and Pharmacology*, 93(10), 893–901. doi:10.1139/cjpp-2014-0474.

White, C.W., Messer, S.J., Large, S.R., et al. (2018). Transplantation of Hearts Donated after Circulatory Death. *Frontiers in Cardiovascular Medicine*, 5, 8. doi:10.3389/fcvm.2018.00008.